SCIENTIFIC REP☼RTS

OPEN

Topological states and phase transitions in Sb_2Te_3-GeTe multilayers

Thuy-Anh Nguyen[1], Dirk Backes[1], Angadjit Singh[1], Rhodri Mansell[1], Crispin Barnes[1], David A. Ritchie[1], Gregor Mussler[2], Martin Lanius[2], Detlev Grützmacher[2] & Vijay Narayan[1]

Topological insulators (TIs) are bulk insulators with exotic 'topologically protected' surface conducting modes. It has recently been pointed out that when stacked together, interactions between surface modes can induce diverse phases including the TI, Dirac semimetal, and Weyl semimetal. However, currently a full experimental understanding of the conditions under which topological modes interact is lacking. Here, working with multilayers of the TI Sb_2Te_3 and the band insulator GeTe, we provide experimental evidence of multiple topological modes in a single Sb_2Te_3-GeTe-Sb_2Te_3 structure. Furthermore, we show that reducing the thickness of the GeTe layer induces a phase transition from a Dirac-like phase to a gapped phase. By comparing different multilayer structures we demonstrate that this transition occurs due to the hybridisation of states associated with different TI films. Our results demonstrate that the Sb_2Te_3-GeTe system offers strong potential towards manipulating topological states as well as towards controlledly inducing various topological phases.

Topological surface modes

Topological insulators (TIs) are a recently emerged class of materials which are insulating in the bulk, but whose surface harbours 'topologically protected' conducting modes[1]. The existence of the topological surface modes (TSMs) stems ultimately from the high spin-orbit coupling in TIs which 'inverts' the conduction and valence bands. In other words, the band structure of the TI is topologically distinct from the ordinary band insulator (BI) and the TSMs arise because the band gap *must* close at a TI-BI interface, or even an interface between a TI and the vacuum[2]. Importantly, local perturbations (e.g., disorder) which do not alter the topological properties of the system cannot localise the TSMs, and this gives rise to their 'topological protection'. The TSMs have various exotic properties such as a linear *Dirac*-like dispersion, and a well-defined helicity, i.e., spin and momentum vectors at fixed angles to each other. These properties render them useful in a variety of settings such as low-power electronics and spin-based communication and computation. In addition, when TSMs couple to each other they are predicted to produce a very diverse phase diagram of novel topological phases[3–5]. In particular, in ref. 3 it was first proposed that superlattices of alternating TI and BI layers can overall either be TIs or BIs depending on the specifics of how the TSMs couple, and under certain conditions be Weyl semimetals[6]. Experimentally, there have been reports of TIs in superlattice structures including PbSe-Bi_2Se_3 structures[7,8], $Bi_14Rh_3I_9$[9], and Sb-Te binary systems[10,11], although the crucial aspect of how the TSMs couple across the intervening layers remains unexplored. In this manuscript we investigate the low-temperature (low-*T*) electrical properties of molecular beam epitaxy (MBE)-grown bi-layer and tri-layer structures of Sb_2Te_3, a well-known TI[12], and GeTe, a narrow band gap semiconductor that goes superconducting at very low *T*[13,14]. Intriguingly, our results indicate two-dimensional (2D) transport, indicating that the structures are dominated by the Sb_2Te_3-GeTe interface. Remarkably, we realise specific situations in which the tri-layer system has either a *quadratically dispersive* mode or *three linearly dispersive* Dirac-like modes. Based on very simple assumptions we argue that the two states are topologically distinct, thus suggesting Sb_2Te_3-GeTe heterostructures to be promising platforms to induce topological phase transitions and also realise multi-TSM systems[3,4,15].

TSMs in TIs have been most clearly identified using angle-resolved-photoemission-spectroscopy[16,17], although this technique is unable to probe the interior of materials, and thus has limited applicability in studying buried

[1]Cavendish Laboratory, Department of Physics, University of Cambridge, J. J. Thomson Avenue, Cambridge CB3 0HE, United Kingdom. [2]Peter Grünberg Institute (PGI-9), Forschungszentrum Jülich, 52425 Jülich, Germany. Correspondence and requests for materials should be addressed to V.N. (email: vn237@cam.ac.uk)
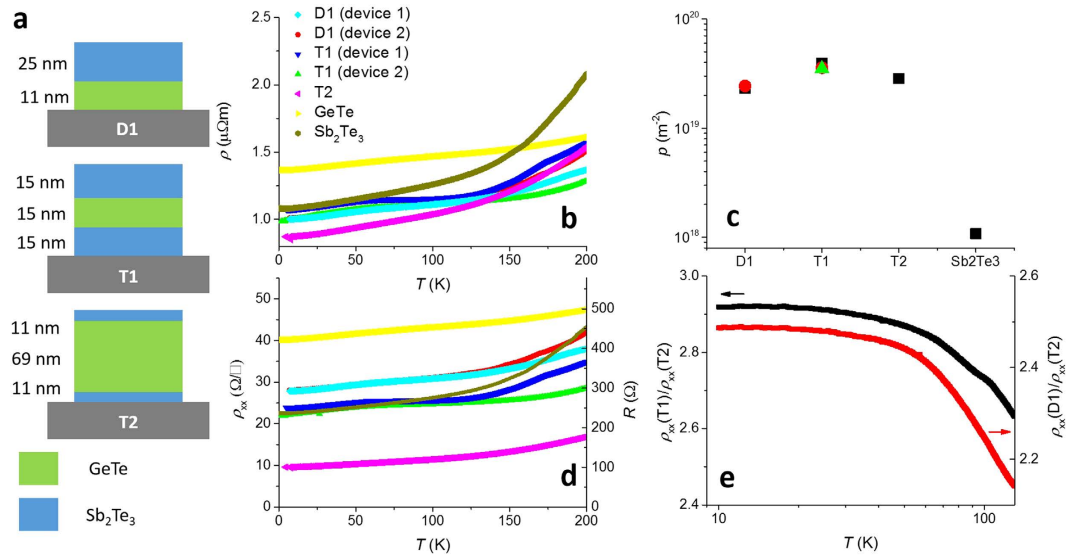
Figure 1. The multilayer structures that are investigated are schematically depicted in (**a**). In (**b**) we show the T-dependence of ρ where, intriguingly, it is seen that the heterostructures have a lower ρ than both of the parent materials. (**c**) The carrier concentrations in the multilayers are more than an order of magnitude greater than that of pure Sb_2Te_3 and this is a direct outcome of the proximity to the larger bandgap material GeTe. (measurements from multiple samples are shown for D1 and T1). In (**d**) the data shown in (**b**) is plotted as a 2D resistivity ρ_{xx}. The right axis shows the measured resistance R. (**e**) Shows the ratio of ρ_{xx} in T1 and T2 to be ≈ 2.9, and that of D1 and T2 to be ≈ 2.5 at low T.

TSMs in structures of the type we report. Electrically, TSMs can be identified by observing quantum corrections to the conductivity σ at low T. The strong spin-orbit interaction in TIs engenders positive quantum corrections to σ in the form of weak antilocalization (WAL) at low T[18] which manifests as a characteristic cusp in the magnetoresistance described by the Hikami-Larkin-Nagaoka (HLN) equation[18]:

$$\Delta\sigma_{xx}^{2D} \equiv \sigma_{xx}^{2D}(B_\perp) - \sigma_{xx}^{2D}(0) = \alpha\frac{e^2}{2\pi^2\hbar}\left[\ln\left(\frac{\hbar}{4eB_\perp\ell_\varphi^2}\right) - \Psi\left(\frac{1}{2} + \frac{\hbar}{4eB_\perp\ell_\varphi^2}\right)\right]$$

(1)

Here σ_{xx} indicates the longitudinal component of conductivity and the superscript 2D indicates that the equation is valid for a two-dimensional conducting sheet, $B_\perp$ is the magnetic field perpendicular to the 2D plane, α is a parameter $= 0.5$ for each 2D WAL channel, e is the electronic charge, $\hbar$ is Planck's constant divided by 2π, ℓ_φ is the phase coherence length, and Ψ is the digamma function. In TI thin films it is expected that $\alpha = 1$ due to the top and bottom surfaces, although often transport measurements in TI thin films are consistent with $\alpha \approx 0.5$, i.e., the existence of a single TSM[19]. There is a growing consensus that this is due to the interfacial disorder between the TI and substrate which destroys the bottom TSM. Importantly, this hinders progress towards understanding the interaction between TSMs. As an alternative, exfoliated TI structures have been used[20] which are significantly less prone to interfacial disorder, but offer considerably less control over the film thickness. In this context, therefore, our approach of utilising MBE-grown multilayers is particularly promising in that it potentially overcomes both these limitations.

Results and Discussion

The wafer structures that we report here are schematically represented in Fig. 1a. The first is a double-layer structure with 11 nm of GeTe capped by 25 nm of Sb_2Te_3, henceforth referred to as D1. The second and third are three-layer Sb_2Te_3-GeTe-Sb_2Te_3 sandwich structures which we refer to as T1 and T2, respectively. In T1 each of the three layers is 15 nm thick, and T2 consists of a relatively thick 69 nm GeTe layer between 11 nm Sb_2Te_3 layers. The lattice mismatch of $\approx 2.5\%$ between Sb_2Te_3 and GeTe is small enough to allow for coherent growth (see Methods). In addition, to benchmark our results, we have studied pure Sb_2Te_3 and GeTe films of thickness 48 nm and 34 nm, respectively. Figure 1b shows the resistivity P vs T of Hall bar devices fabricated from the different wafers. The first important fact to note is that, surprisingly, the multilayer structures are *consistently less resistive* than the pure samples, and closer in resistivity to Sb_2Te_3. Especially noteworthy in this context is that T2, which has the largest relative proportion of GeTe ($\approx 76\%$), has the lowest ρ and shows the strongest deviation from pure GeTe. These observations clearly indicate that the individual layers do not behave simply as independent resistors connected in parallel, but rather interact with each other. One possibility is that the band bending at the interface between GeTe (band gap ≈ 0.65 eV[21]) and Sb_2Te_3 (band gap ≈ 0.2 eV[22]) serves to draw and confine additional charge carriers into Sb_2Te_3, and thus enhance its conductivity. This notion is corroborated by the measured areal carrier densities in D1, T1 and T2 being over an order of magnitude greater than in Sb_2Te_3 (Fig. 1c). Here we consider the areal rather than bulk carrier density since at low T the conduction in Sb_2Te_3 is largely through the
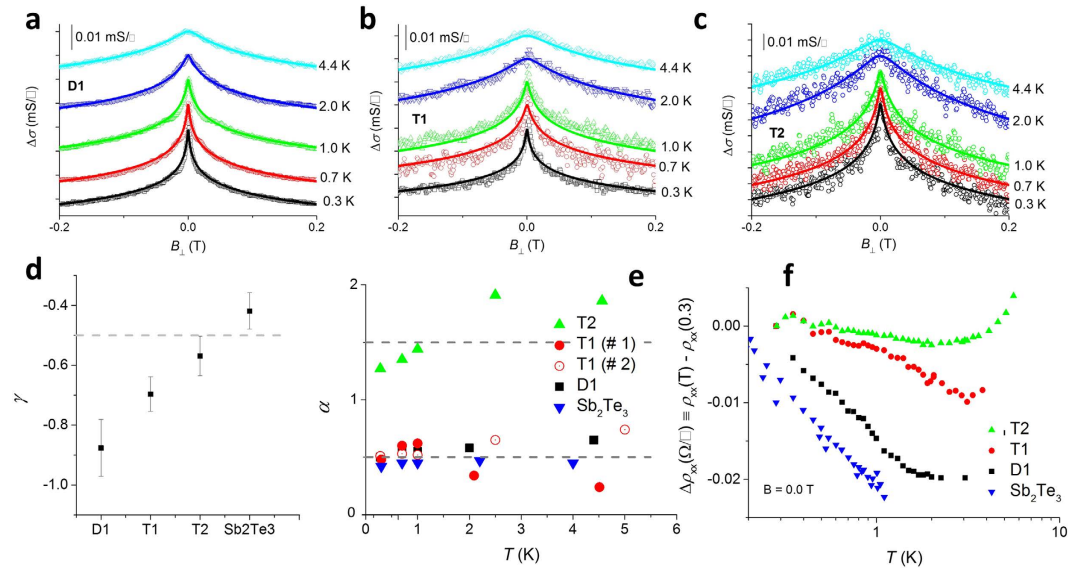
Figure 2. (**a–c**) Show the WAL characteristics for D1, T1 and T2, respectively. Also shown are fits to the HLN formula (Equation 1). The traces are offset vertically for clarity. In (**d**) we observe that the rate of decoherence in T2 and Sb_2Te_3 is consistent with that expected due to inter-particle interactions, whereas in D1 and T1 the rate of decoherence is higher. (**e**) The parameter α which is a measure of the number of WAL channels contribute to the transport is seen to be 0.5 (corresponding to 1 WAL channel) for all the wafers except T2 in which α is approximately 1.5, suggesting the presence of three 2D WAL channels. (**f**) At low-T all the wafers show a logarithmic increase in ρ_{xx} as is expected in 2D systems. It is conceivable that in T1 and T2 GeTe is showing hints of superconductivity at $\approx 0.35\,K$, but this is unlikely to influence the transport unless T is reduced significantly.

TSMs and thus expected to be two-dimensional (2D)[12]. As a reference, the bulk carrier concentration in GeTe was measured to be $\approx 5.5 \times 10^{26}\,m^{-3}$ which, when scaled by the thickness of GeTe is $\sim 10^{19}\,m^{-2}$, is comparable with D1, T1 and T2. In Fig. 1d we plot the 2D resistivity $\rho_{xx} \equiv \rho \times t$, where t is the thickness of the film, as a function of T: in order of increasing ρ_{xx} we find T2, followed by T1 and Sb_2Te_3 which are very similar below $\approx 100\,K$, followed by D1 and then GeTe. The strong dissimilarity between the characteristics of T1 and T2 suggests that there is more physics underlying the heterostructures than just band bending. We return to this fact after having inspected the low T electrical characteristics.

In Fig. 2a–c we show the low-field magnetoconductivity $\sigma_{xx} \equiv \rho_{xx}/(\rho_{xx}^2 + \rho_{xy}^2)$ of D1, T1 and T2, respectively, and observe a pronounced cusp-like minimum around $B_\perp = 0\,T$. Here ρ_{xy} is the Hall resistivity. The signal, expectedly, is not consistent with bulk WAL (see Supplementary Figure S1) where $\Delta\sigma_{xx} \equiv \sigma_{xx}(B_\perp) - \sigma_{xx}(0) \sim B_\perp^{1/2}$ [23], but instead is very well-described by the HLN formula (Equation 1) with α and ℓ_φ as fit parameters. We find that ℓ_φ decays as a power law $\sim T^{-\gamma}$ where the exponent γ is plotted in Fig. 2d. Apart from Sb_2Te_3 and T2, all the structures are observed to undergo decoherence significantly faster than the $\gamma = 0.5$ expected in 2D Nyquist scattering due to inter-particle interactions[24]. Figure 2e shows that α is ≈ 0.5 for Sb_2Te_3, T1 and D1, but is ≈ 1.5 for T2 (see Supplementary Figure S2 for error estimates on α). Recalling that α gets a contribution of 0.5 for each 2D WAL state, we conclude that Sb_2Te_3, T1 and D1 have one 2D mode each while T2 has *three*. While this is consistent with T2 being the least resistive sample under investigation (Fig. 1), there are two important points to consider: First, as discussed earlier in the manuscript, it is expected that $\alpha \approx 0.5$ for Sb_2Te_3 since the TSM at the substrate interface is destroyed. However, unexpectedly we find that even in D1, in which the Sb_2Te_3 film is grown on a well-lattice-matched MBE-grown GeTe film, a second TSM is *not* observed. Second, the occurrence of three 2D modes in T2 agrees with the three TI-BI interfaces (apart from the TI-substrate interface), but this is in apparent contradiction with the observation of only one 2D mode in T1. In a previous study it was found that bare GeTe thin films with $t = 34\,nm$ have $\alpha \approx 1$ [14], i.e., one WAL mode on each side of the film, but GeTe has been intentionally omitted from this plot since it shows superconducting correlations below $T \approx 1.5\,K$ which strongly influence the HLN fits[14].

In the following we investigate the precise role played by GeTe in these heterostructures. First, in order to check whether the tendency of GeTe to become superconducting at very low T has any influence on the transport properties of the multilayer structures we inspect the T-dependence of ρ_{xx} for $T < 10\,K$ in Fig. 2f. We find clearly that $d\rho_{xx}/dT$ is negative below $\approx 3\,K$, qualitatively similar to bare Sb_2Te_3 and in strong agreement with our hypothesis that transport in the multilayers is largely confined to Sb_2Te_3. There may be a maximum in T1 and T2 around $0.35\,K$, but even if this does signal the onset of superconductivity, it is unlikely that this perceptibly affects the transport. Indeed, within the picture that the band gaps of Sb_2Te_3 and GeTe conspire to inject charges from the latter to the former, it is evident why superconductivity is not observed in these samples: the superconducting temperature T_c of GeTe is a monotonically increasing function of its carrier concentration[13] and thus reducing the chemical potential in GeTe, as is achieved when placing it in close proximity to Sb_2Te_3, will only further suppress
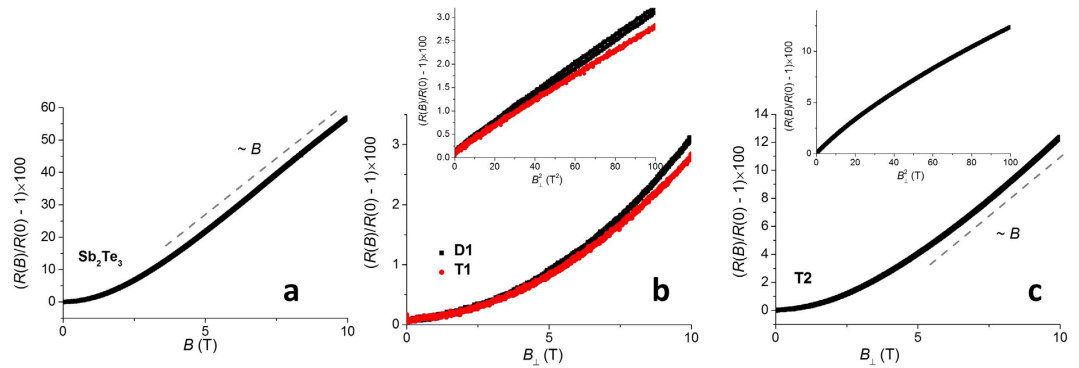
Figure 3. The high-field magnetoresistance of Sb_2Te_3 (**a**) and T2 (**c**) is qualitatively different from D1 and T1 (**b**), with the latter being quadratic in $B_\perp$ over the entire field range explored. Moreover, it is observed in (**b**) that the magnetoresistance characteristics of D1 and T1 are almost identical, thus suggesting similar underlying physics. The insets in (**b,c**) show the magnetoresistance as a function of $B_\perp^2$, clearly bringing out the contrasting behaviours of T1/D1 when compared to T2. The observed linear magnetoresistance in Sb_2Te_3 and T2 is a commonly observed feature in materials with a linear dispersion relation.

T_c. At the typical carrier concentrations obtained in the bare GeTe samples $T_c \approx 0.1\,K$[14], and this essentially precludes the possibility of observing superconductivity at the temperatures our experiments are performed at ($\geq 0.3\,K$). Yet, the strong variation of ρ_{xx} between the different multilayer structures clearly indicates that GeTe is not playing a passive role in the transport. This is especially seen in the contrast between the tri-layer structures T1 and T2: it is seen that $\rho_{xx}(T1) \approx 3\rho_{xx}(T2)$, corresponding almost exactly with the ratio of the number of 2D modes as given by the HLN formula (Fig. 1d). Since the data are clearly indicative of missing WAL modes in T1, we conjecture that certain TSMs in the measured heterostructures hybridise[25,26] and become *gapped*. Importantly, this mechanism would undermine their topological nature and modify the 2D band dispersion from being linear, Dirac-like, to being parabolic near the band minimum.

To investigate the proposed scenario further we study the high-field magnetoresistance characteristics. Figure 3a exemplifies a commonly observed feature in TIs (or Dirac materials, to be more precise), namely a large and *linear* magnetoresistance[19,27–29]. There are various circumstances which can effect such behaviour including very large carrier concentrations[19], transport in 'heavily' disordered conductors[30], and the exclusive occupancy of the lowest Landau level[31,32]. The first two of these are not applicable to our experimental system since the carrier concentration, which is similar between the multilayers, clearly does not influence the nature of magnetoresistance (Fig. 3), and the level of disorder in MBE-grown films is expected to be small. On the other hand, the third criterion is known to be experimentally more accessible in Dirac materials than those with a parabolic dispersion[19]. That is, in our experimental system we can directly correlate the presence or absence of large, linear magnetoresistance to the presence or not of Dirac-like states. Thus, a critical conclusion we arrive at from Fig. 3(a,b) is that D1 is not, as one would naively expect, simply a TI layer on a lattice-matched, insulating substrate, but has at least one gapped state which dominates the magnetoresistance at high fields. Since the Sb_2Te_3 layer is significantly thicker than 6 nm, the approximate thickness below which the top and bottom TSMs are known to hybridise in Sb/Bi-based TIs[25,33,34] it is unlikely that the top TSM has developed a gap. Which then implicates the lower TSM, but raises the question as to what it hybridises with. Recalling that 34 nm thick GeTe harbours *two* surface states[14], our data strongly points in favour of the 2D modes on either side of the 11 nm thick GeTe layer hybridising with each other. This is also consistent with the fact that T1 has only one 2D WAL mode where, as per the previous arguments, the two embedded TSMs hybridise across the 15 nm thick GeTe layer. This idea is firmly reinforced by the data in Fig. 3b where we find that the magnetoresistance of D1 and T1 agree *quantitatively*, thus indicating similar underlying physics. Of particular interest in this regard is the fact that in T1, both hybridising states are topological in nature, but in D1, the bottom state is necessarily not topological (but Dirac-like[35]). The hybridisation picture also provides an estimate of the wavefunction extent outward from the interface. Since hybridisation is possible across a 15 nm thick GeTe layer, we can conclude that the wavefunctions on either side have significant overlap and therefore must have a spatial extent of $\geq 7.5\,nm$. Clearly, however, the wavefunction is not symmetric about the GeTe-Sb_2Te_3 interface since its extent in Sb_2Te_3 is $\leq 5.5\,nm$. Such asymmetry is not unexpected being dependent on factors such as the band offsets between the different materials and precise form of the interface confining potential.

The conclusion that the buried TSMs in T1 hybridise across the GeTe layer can also be arrived at by contrasting the behaviours of T1 and T2: Fig. 2e suggests that none of the TSMs in T2 hybridise and this is buttressed by the observation in Fig. 3c that ρ_{xx} vs $B_\perp$ is linear above $\approx 5\,T$. Therefore, since the TSMs flanking the Sb_2Te_3 layer in T2 do not hybridise, they must not in T1 either where the Sb_2Te_3 layers are thicker. Thus the only possibility is that we are observing the hybridisation of TSMs across the GeTe layer, i.e., between TSMs associated with *different* TI layers. To the best of our knowledge this is the first experimental demonstration of hybridisation between TSMs not related by symmetry. More importantly, our data evidences a critical thickness of GeTe at which the Sb_2Te_3-GeTe-Sb_2Te_3 heterostructure undergoes a topological phase transition, thus indicating it to be a promising system in which to study topological phase transitions[15,36–38].

But then what of the remaining TSM on the top surface of D1 and T1? Being gapless, this mode will dominate the low T transport characteristics, but the high-field transport will be dominated by the non-Dirac-like modes which have a dramatically lower magnetoresistance. Notably, it was shown in ref. 39. that the size of the WAL effect should reduce as the gap in the surface states widens relative to the Fermi energy, i.e, we do not expect the gapped states to contribute significantly to the measured WAL. In this context, Fig. 1e where we find the ratios $\rho_{xx}(T1)/\rho_{xx}(T2)$ and $\rho_{xx}(D1)/\rho_{xx}(T2)$ to be constant below $T \approx 30$ K, sheds light on the relevant energy scales. Both the ratios are ~3, consistent with the ratio of the number of 2D modes. This temperature scale corresponds to ≈ 2.6 meV, which is two orders of magnitude smaller than the band gap of Sb_2Te_3, and thus the decrease in $\rho_{xx}(T1)/\rho_{xx}(T2)$ and $\rho_{xx}(D1)/\rho_{xx}(T2)$ with increasing T most likely corresponds to the activation of the hybridised TSMs. We, therefore, have obtained a crude measure of the hybridisation gap to be about 2.6 meV. Not only does this provide an experimentally measured parameter useful for simulations of TI-BI superlattices, it also shows the experimental system to be a versatile platform to realise and manipulate multiple TSMs. In conclusion, we have demonstrated a phase transition in the topological properties of Sb_2Te_3-GeTe-Sb_2Te_3 structures as the thickness of the GeTe layer is varied. We have demonstrated this system to be a close realisation of the model proposed by Burkov and Balents[3] to induce novel topological phases. We have provided the first experimental demonstration of hybridisation between TSMs associated with different TIs and shown the experimental system to be potentially exploitable in applications requiring multiple TSMs in parallel.

Experimental Section

Thin film growth.   The GeTe and Sb_2Te_3 films were grown on Si(111) wafers using MBE. Before the deposition, the Si substrates were cleaned by the HF-last RCA procedure to remove the native oxide and passivate the surface with hydrogen. Subsequently, the substrates were heated *in-situ* at 750 °C for 20 min to desorb hydrogen atoms from the surface. The Ge, Sb, and Te material fluxes were generated by effusion cells with temperatures of 1250 °C, 440 °C, and 330 °C, respectively. For all samples the Te shutter was opened 2 seconds before the Ge or Sb shutter in order to saturate the Si substrate surface with Te. During the entire growth process the substrate was set at 280 °C. The lattice parameters of Sb_2Te_3 and GeTe are, respectively, $a_{Sb_2Te_3} = 4.26$ Å and $a_{GeTe} = 8.32$ Å, and thus the lattice mismatch at 2:1 correspondence is $(2 \times a_{Sb_2Te_3} - a_{GeTe})/a_{GeTe} = 2.5\%$.

Device fabrication and electrical measurements.   We used photolithography and argon ion milling to fabricate Hall bar devices of dimensions 100 μm × 1050 μm, after which Ti/Au ohmic contacts were deposited using a lift-off process. The devices were packaged and measured in a He 3 cryostat with a base $T = 280$ mK, and equipped with a 10 T superconducting magnet. Resistance and Hall measurements were made in a standard four-terminal setup with an excitation current $I_{ex} = 0.1 - 1\ \mu$A at frequency $f = 17$ Hz.

Data availability.   Supporting data for this paper is available at the DSpace@Cambridge data repository (http://dx.doi.org/10.17863/CAM.16)

References

1. Hasan, M. & Kane, C. Topological insulators. *Rev. Mod. phys.* **82,** 3045 (2010).
2. Moore, J. The birth of topological insulators. *Nature* **464,** 194 (2010).
3. Burkov, A. & Balents, L. Weyl semimetal in a topological insulator multilayer. *Phys. Rev. Lett.* **107,** 127205 (2011).
4. Li, X., Zhang, F., Niu, Q. & Feng, J. Superlattice valley engineering for designer topological insulators. *Sci. Rep.* **4,** 6397 (2014).
5. Owerre, S. Weyl semimetal in ultra-thin film of topological insulator multilayer. http://arxiv.org/abs/1601.03707 (2016).
6. Hasan, M., Xu, S.-Y. & Bian, G. Topological insulators, topological superconductors and Weyl fermion semimetals: discoveries, perspectives and outlooks. *Phys. Scripta* **T164,** 014001 (2015).
7. Nakayama, K. *et al.* Manipulation of topological states and the bulk band gap using natural heterostructures of a topological insulator. *Phys. Rev. Lett.* **109,** 236804 (2012).
8. Sasaki, S., Segawa, K. & Ando, Y. Superconductor derived from a topological insulator heterostructure. *Phys. Rev. B (R)* **90,** 220504 (2014).
9. Rasche, B. *et al.* Stacked topological insulator built from bismuth-based graphene sheet analogues. *Nat. Mater.* **12,** 422 (2013).
10. Takgaki, Y., Giussani, A., Tominaga, J., Jahn, U. & Calarco, R. Transport properties in a Sb-Te binary topological-insulator system. *J. Phys.: Condens. Matter.* **25,** 345801 (2013).
11. Takagaki, Y., Jahn, U., Giussani, A. & Calarco, R. Multiple state transport deduced by weak antilocalization and electron-electron interaction effects in Sb_xTe_{1-x} layers. *J. Phys.: Condens. Matter* **26,** 095802 (2014).
12. Zhang, H. *et al.* Topological insulators in Bi_2Se_3, Bi_2Te_3 and Sb_2Te_3 with a single dirac cone on the surface. *Nat. Phys.* **5,** 438 (2009).
13. Hein, R. A., Gibson, J. W., Mazelsky, R., Miller, R. C. & Hulm, J. K. Superconductivity in germanium telluride. *Phys. Rev. Lett.* **12,** 320 (1964).
14. Narayan, V., Nguyen, T.-A., Mansell, R., Ritchie, D. & Mussler, G. Interplay of spin-orbit coupling and superconducting correlations in germanium telluride thin films. *Phys. Status Solidi RRL* **10,** 253 (2016).
15. Tominaga, J., Kolobov, A. V., Fons, P., Nakano, T. & Murakami, S. Ferroelectric order control of the dirac-semimetal phase in GeTe-Sb_2Te_3 superlattices. *Adv. Mater. Interfaces* **1,** 1300027 (2014).
16. Hsieh, D. *et al.* A topological Dirac insulator in a quantum spin hall phase. *Nature* **452,** 970 (2008).
17. Hsieh, D. *et al.* Observation of unconventional quantum spin textures in topological insulators. *Science* **323,** 919 (2009).
18. Hikami, S., Larkin, A. I. & Nagaoka, Y. Spin-orbit interaction and magnetoresistance in the two-dimensional random system. *Prog. Theor. Phys.* **63,** 707 (1980).
19. Veldhorst, M. *et al.* Magnetotransport and induced superconductivity in Bi based three-dimensional topological insulators. *Phys. Status Solidi RRL* **7,** 26 (2013).
20. Checkelsky, J., Hor, Y., Cava, R. & Ong, N. Bulk band gap and surface state conduction observed in voltage-tuned crystals of the topological insulator Bi_2Se_3. *Phys. Rev. Lett.* **106,** 196801 (2011).
21. Di Sante, D., Barone, P., Bertacco, R. & Picozzi, S. Electric control of the giant Rashba effect in bulk GeTe. *Adv. Mater.* **25,** 509 (2013).
22. Madelung, O., Rössler, U. & Schulz, M. O. *Antimony telluride (Sb_2Te_3) band structure, energy gap in Non-Tetrahedrally Bonded Elements and Binary Compounds I* (Springer-Verlag, Berlin Heidelberg 1998).
23. Kawabata, A. Theory of negative magnetoresistance i. application to heavily doped semiconductors. *Journ. Phys. Soc. Japan* **49,** 628 (1980).

24. Altshuler, B., Tagliacozzo, A. & Tognetti, V. *Quantum phenomena in mesoscopic systems* (IOS Press, Amsterdam 2003).
25. Zhang, Y. *et al.* Crossover of the three-dimensional topological insulator Bi$_2$Se$_3$ to the two-dimensional limit. *Nat. Phys.* **6,** 584 (2010).
26. Murakami, S. *"Hybridization of Topological Surface States and Emergent States,"* in *Topological Insulators: Fundamentals and Perspectives* (Wiley-VCH Verlag GmBH & Co. KGaA, Weinheim, Germany 2015).
27. Qu, D.-X., S, H. Y., Xiong, J., Cava, R. & Ong, N. Quantum oscillations and hall anomaly of surface states in the topological insulator Bi$_2$Te$_3$. *Science* **329,** 821 (2010).
28. Tang, H., Liang, D., Qiu, R. L. J. & Gao, X. P. A. Two-dimensional transport-induced linear magneto-resistance in topological insulator Bi$_2$Se$_3$ nanoribbons. *ACS Nano* **5,** 7510 (2011).
29. Wang, X., Du, Y., Dou, S. & Zhang, C. Room temperature giant and linear magnetoresistance in topological insulator Bi$_2$Te$_3$ nanosheets. *Phys. Rev. Lett.* **108,** 266806 (2012).
30. Parish, M. & Littlewood, P. Non-saturating magnetoresistance in heavily disordered semiconductors. *Nature* **426,** 162 (2003).
31. Abrikosov, A. Galvanometric phenomena in metals in the quantum limit. *Sov. Phys. JETP* **29,** 746 (1969).
32. Abrikosov, A. Quantum magnetoresistance. *Phys. Rev. B* **58,** 2788 (1998).
33. Li, Y.-Y. *et al.* Intrinsic topological insulator Bi$_2$Se$_3$ thin films on si and their thickness limit. *Adv. Mater.* **22,** 4002 (2010).
34. Jiang, Y. *et al.* Landau quantization and the thickness limit of topological insulator thin films of Sb$_2$Te$_3$. *Phys. Rev. Lett.* **108,** 016401 (2012).
35. Krempaský, J. *et al.* Surface versus bulk contributions to the giant Rashba splitting in the ferroelectric α-GeTe(111) semiconductor. http://arxiv.org/abs/1503.05004 (2016).
36. Kim, J., Kim, J. & Jhi, S.-H. Prediction of topological insulating behavior in crystalline Ge-Sb-Te. *Phys. Rev. B (R)* **82,** 201312 (2010).
37. Sa, B., Zhou, J., Sun, Z., Tominaga, J. & Ahuja, R. Topological insulating in GeTe/Sb$_2$Te$_3$ phase-change superlattice. *Phys. Rev. Lett.* **109,** 096802 (2012).
38. Kim, J., Kim, J., Kim, K.-S. & Jhi, S.-H. Topological phase transition in the interaction of surface dirac fermions in heterostructures. *Phys. Rev. Lett.* **109,** 146601 (2012).
39. Lu, H.-Z., Shi, J. & Shen, S.-Q. Competition between weak localization and antilocalization in topological surface states. *Phys. Rev. Lett.* **179,** 076801 (2011).

Acknowledgements

Author Contributions

T.-A.N., D.B. and V.N. performed the experiments, T.-A.N., D.B., R.M. and A.S. fabricated the devices, G.M., M.L. and D.G. grew the samples, V.N. wrote the paper with inputs from R.M., G.M., D.B. and T.-A.N. All the authors reviewed the manuscript.

Additional Information

Supplementary information accompanies this paper at http://www.nature.com/srep

Competing financial interests: The authors declare no competing financial interests.

How to cite this article: Nguyen, T.-A. *et al.* Topological states and phase transitions in Sb$_2$Te$_3$-GeTe multilayers. *Sci. Rep.* **6,** 27716; doi: 10.1038/srep27716 (2016).